

# Development of Material Databases and Volume Heat Source for Temper Bead Welding Process

Jangho Ahn<sup>a\*</sup>, Won Geun Yi<sup>b</sup>, Sung Bu Choi<sup>c</sup>

<sup>a</sup>ESI Korea Co., LTD, 4F Ryuhsan Bldg. 134-1 Gayang-Dong, Gangseo-Gu, Seoul Korea

<sup>b</sup>Doosan Heavy Industries & Construction, 22 DoosanVolvo-ro, Seongsan-gu, Changwon, Gyeongnam, Korea

<sup>c</sup>Korea Institute of Nuclear Safety, 62 Gwahak-ro, Yuseong-gu, Daejeon Korea

\*Corresponding author: [ajh@esi-group.com](mailto:ajh@esi-group.com)

## 1. Introduction

Occurrences of Primary Water Stress Corrosion Cracking (PWSCC) of Alloy 600 material used for reactor vessel head penetrations of Davis Besse (USA) and steam generator bowl drain nozzle of Hanbit #3, #4 nuclear power plants have been increased. Therefore, nuclear licensee, manufacturer and maintenance companies have been developing various weld repair and mitigation techniques for components which PWSCC was occurred. Two applications of topical reports which related to those repair and mitigation techniques have been submitted and are under review process. Temper Bead Welding (TBW) is one of the repairing techniques applicable to nuclear power plants. Post Weld Heat Treatment (PWHT) process for carbon steels and low alloyed steels is required for removal of residual stresses and diffusible hydrogen contents and for toughness improvement of heat affected zone after welding process. But in case of repairing for NPP components are under operation, PWHT process is difficult to be applied and TBW has been adopted in alternative techniques of PWHT process recently in USA and other countries.

To model thermal and metallurgical behaviors with finite element analysis of carbon steels and low alloyed steel under TBW process, it is important to develop a material database which take account into solid state phase transformation phenomena and model a precise volume heat source for welding process.

In this study, the development of solid state phase transformation material database take account into TTT and CCT diagrams and volume heat source to match precisely with experimental results from TBW have been conducted.

## 2. Methods and Results

Single pass bead on plate specimens were prepared as shown in Fig. 1. For base material, SA-516 Gr. 70 (P-No. 1) was used and ERNiCrFe-7A (F-No.43) was used for wire material.

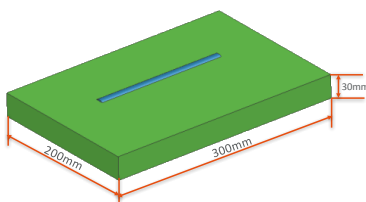
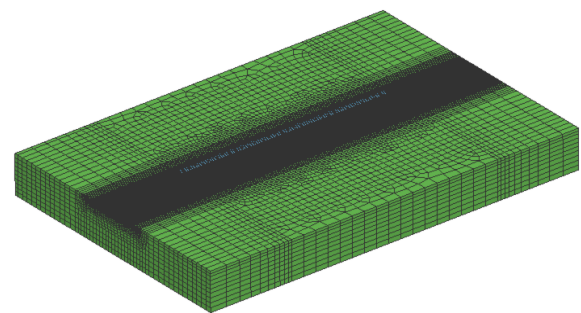
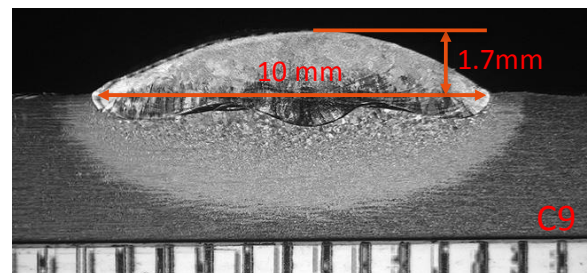


Figure. 1. Geometry of single pass bead on plate specimen.

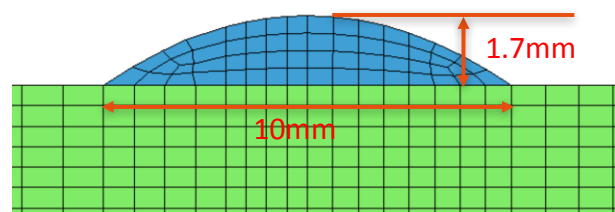
A 3D finite element model for conducting heat source fitting and validation analysis was created based on measured geometry from the welding specimens and shown in Fig. 2.



a) 3D Fe model



b) Measured geometry of bead area



c) Finite element model of bead area

Figure. 2. 3D FE model and comparison between measured and FE model of bead area.

### 2.1. Development of material database

In the case of a low alloyed carbon steel, the metallurgical transformations to be described are principally the diffusion controlled transformation which austenitic, ferritic, pearlitic, bainitic during heating and cooling and the martensitic transformations which is time independent transformation during cooling. To model diffusion controlled transformation, Kolmogorov-Johnson-Mehl-Avrami (KJMA) equation

has been used by many authors to describe phase fraction change [1, 2]. KJMA model can be calibrated with Time Temperature Transformation (TTT) diagram based on isothermic transformation kinetic or Continuous Cooling Transformation (CCT) diagram based on non isothermic transformation kinetics. For welding applications, the operating conditions are practically always one of rapid heating (application of heat input) or rapid cooling. Therefore, it is possible to fit KJMA equation only using Continuous Cooling Transformation (CCT) diagram but to obtain best accurate calibration, both TTT and CCT diagram are required [3].

In this study, KJMA equation was calibrated with TTT and CCT diagrams for SA-516 Gr. 70 alloy. TTT and CCT diagrams was calculated from thermo-dynamic software. Calibration of KJMA equation with TTT and CCT diagrams was conducted by PTCM manager which provided by SYSWELD software [3]. First, values (starting time, end time and maximum phase proportion of each phases at various temperatures) taken from TTT diagrams are needed to calibrate temperature dependent values such as time delay function ( $\tau$ ) and exponent ( $n$ ) in KJMA equation. In Fig. 3, input values from TTT diagram and calculated values for Ferrite/Pearlite phase of SA-516 Gr. 70 alloy are shown.



Figure 3. TTT diagram fitting for Ferrite/Pearlite phase of SA-516 Gr. 70 alloy.

Next, to calibrate cooling rate dependent values for non isothermal cooling conditions, cooling rates and final phase proportions of each phases taken from CCT diagram were inputted in PTCM manager as shown in Fig. 4.

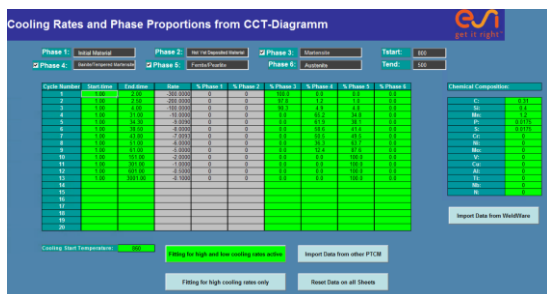


Figure 4. CCT diagram fitting of SA-516 Gr. 70 alloy.

For martensitic phase transformation, Martensitic transformation is independent of time. The proportion of martensite formed depends only on the temperature and is well described by Koistinen– Marbürger’s law [4]. Calibration of values, martensite start temperature ( $M_s$ ) and  $b$  in Koistinen– Marbürger’s law was conducted by PTCM manager using evolution of martensite phase proportion data taken from TTT and CCT diagrams. (Fig. 5.)

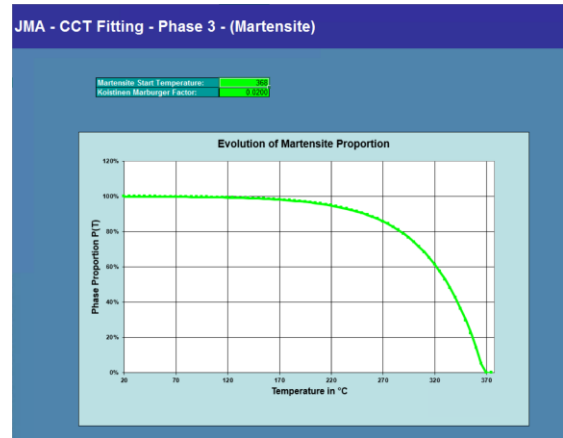
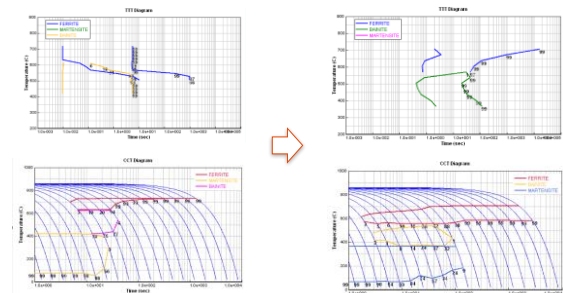


Figure 5. Martensite fitting of SA-516 Gr. 70 alloy.

Comparison between drawn TTT and CCT diagrams based on calibrated KJMA values using CCT only (a) and TTT and CCT diagrams (b) which developed in this study are shown in Fig. 6.



(a) KJMA calibrated using CCT only (b) KJMA calibrated using TTT and CCT

Figure 6. TTT and CCT diagram comparison of different KJMA calibration methods.

## 2.2. Development of volume heat source

In welding simulation, the real physical effects that cause the heat transfer from the power source in the structure are not simulated, because material and process data is rather complex, numerous physical effects are directly coupled and computations are extremely costly. The heat transfer from the welding equipment into the structure is modeled by an analytical heat conduction model. A heat source in the form of two semi-ellipsoids has thus been proposed by Goldak et

al[5] in order to model the heat input associated with arc welding processes with addition of material. Goldak heat source model and energy parameters are shown in Fig. 7.

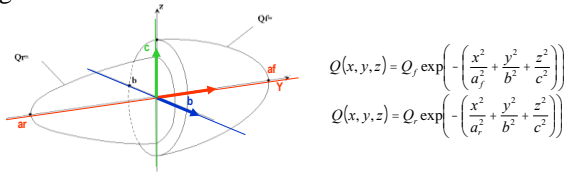


Figure 7. Modeling of Goldak heat source model and energy parameters.

Modeling of heat source model often requires adjustments to experimental data such as shape of molten zone and heat affected zone.

Single bead on plate specimen was prepared with using same welding process condition for TBW and welding process parameters are shown in Table 1.

Average Current	Voltage	Speed	Heat Input
A	V	mm/min	kJ/mm
190	11	85	1.48

Table 1. Welding process conditions for TBW single pass bead on plate specimen.

A macrograph from TBW single bead on plate model is shown in Fig. 8. Width of molten zone is approximately 10mm and penetration depth is 0.95mm.

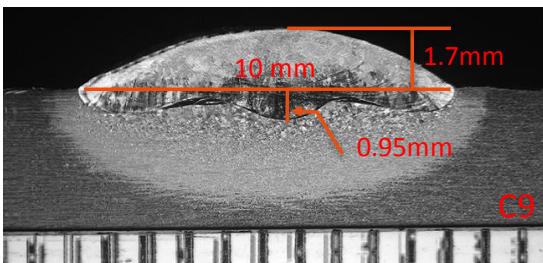


Figure 8. A macrograph from TBW single bead on plate model.

Shape parameters b, c, af and ar in Fig. 7 can be determined by measurement values from Fig. 8. And energy parameters can be determined by heat input values from Table. 1. Initial shape and energy parameters for heat source model for TBW are shown in Table. 2 and location is shown in Fig. 9.

Parameters	Values	Units
Q	2064	W
b	5	mm
c	0.8	mm
af	3.33	mm
ar	6.667	mm

Table 2. Shape and energy parameters of initial heat source model for TBW single pass bead on plate specimen.

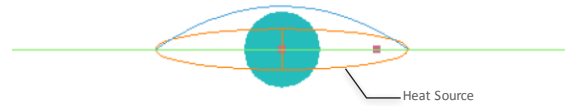


Figure 9. Location of initial heat source TBW single pass bead on plate specimen.

Fig. 10 shows predicted maximum temperature distribution during TBW process using initial heat source parameters. Liquid zone refers to molten zone.

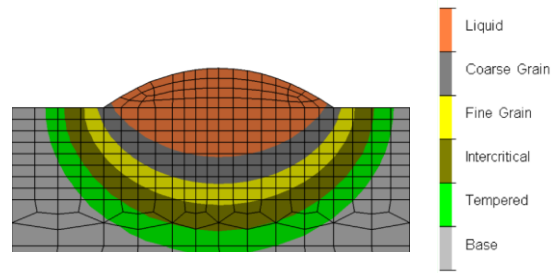


Figure 10. Predicted maximum temperature distribution using initial heat source parameters.

Predicted width of molten zone is close to measured value but penetration depth (approximately 2mm) is bigger.

Changed heat source shape parameters and locations to obtain similar shape of MZ and HAZ are described in Table 3 and the results are shown in Fig. 11.

	b	c	af	ar	Offset	Q
HSF1	5.0	0.8	3.33	6.667	0	2064
HSF2	5.5	0.8	3.33	6.667	0	2064
HSF3	7.5	0.8	3.33	6.667	0	2064
HSF4	15.0	0.8	3.33	6.667	0	2064
HSF5	15.0	0.8	3.33	6.667	0.8	2064
HSF6	3.0	0.8	3.33	6.667	0.8	2064

Table 3. Heat source shape parameters and locations

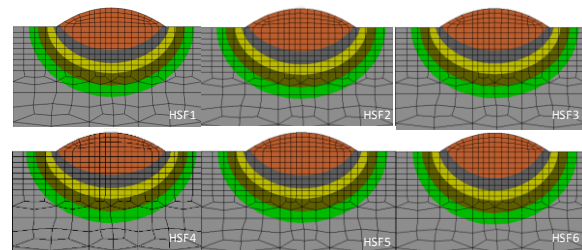


Figure 11. Predicted maximum temperature distribution using initial heat source parameters.

As shown in Fig. 11, width of molten zone and penetration depth are not changed while heat source parameters were changed. This phenomenon can be explained with energy distribution shown in Fig. 12.

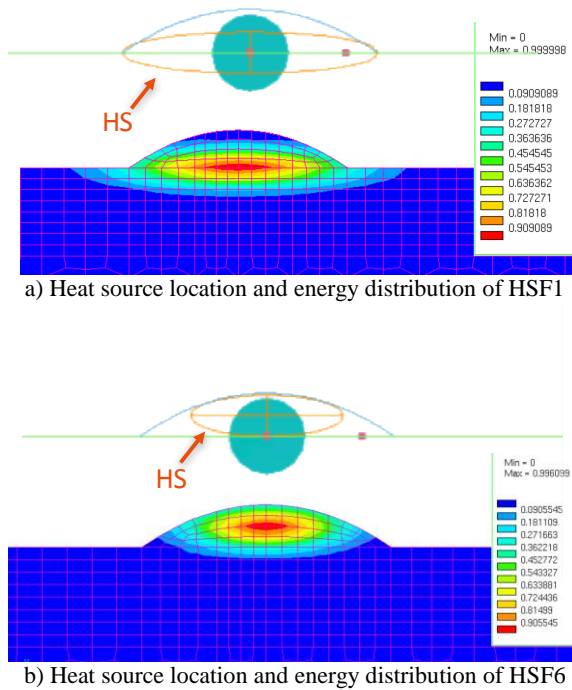


Figure. 12. Energy distributions for different heat source parameters.

Due to gaussian energy distribution of heat source and sum of energy is constant for different heat source shape parameters, high intensity of energy concentrated to center of single heat source and conduction heat transfer to base material created bigger penetration depth.

To create wide molten zone with shallow penetration depth as experimental results, multiple volume heat sources were introduced. Three heat sources which width and powers are divided by 3 from single heat source and predicted results were shown in Fig. 13. But penetration depth is bigger than measured.

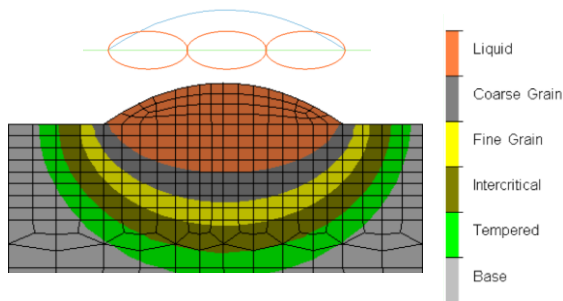


Figure. 13. 3 heat sources shapes and locations and predicted molten zone.

After several iterations on changing heat source shape and energy parameters, best parameters are obtained

and shown in Table 4. and predicted molten zone shape comparison between measured is shown in Fig. 14.

	b	c	af	ar	Offset	Q	
HS-L	1.25	0.8	3.333	6.667	-4	516.1	1714
HS-C	1.25	0.8	3.333	6.667	0	681.3	
HS-R	1.25	0.8	3.333	6.667	4	516.1	

Table. 4. Final heat source shape and energy parameters for multiple heat sources.

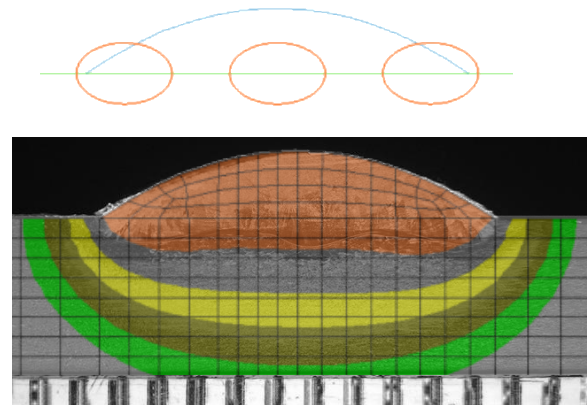


Figure. 14. Location of final multiple heat sources and comparison between measured and predicted molten zone shape.

### 3. Conclusions

Phase transformation calibration using both TTA and CCT diagrams was conducted and create precise material database for SA-516 Gr. 70 alloy. Single pass bead on plate specimen was created using TBW process condition and reproduced molten zone shape using multiple volume heat sources on 3D FE model. Further studies on thermal, metallurgical and mechanical behaviors for multipass TBW specimens with obtained material database and multiple volume heat sources will be carried out.

### REFERENCES

- [1] Li JJ, Wang JC, Xu Q, Yang GC. Comparison of Johnson-Mehl-Avrami-Kolmogorov (JMAK) kinetics with a phase field simulation for polycrystalline solidification. *Acta Materialia*, 55, 825, 2007.
- [2] Inoue T, Arimoto K. Development and implementation of CAE system hearts for heat treatment simulation based on metallo-thermo-mechanics. *Journal of Materials Engineering and Performance*, 6, 51, 1997
- [3] Calibration of Metallurgical Input Data Based on TTT and CCT diagrams, ESI Group
- [4] Koistinen D P and Marburger R E: 'A general equation pre- scribing extend of austenite–martensite transformation in pure Fe–C alloys and plain carbon steels'. *Acta Met*, 7, 59, 1959.
- [5] Goldak J A et al: 'A new finite element model for welding heat sources'. *Metallurgical Transactions* 15B 299–305, 1984.